J Mater Sci (2011) 46:1414–1423
DOI 10.1007/s10853-010-4936-z

Investigation of mechanical, electrical, and thermal properties of a Zn–1.26 wt% Al alloy

Emin Çadırlı · Mevlüt Şahin

Received: 2 June 2010 / Accepted: 17 September 2010 / Published online: 1 October 2010

Abstract Zn–1.26 wt% Al alloy was directionally solidified upward with a constant growth rate ($V = 16.6$ μm/s) in a wide range of temperature gradients (1.94–5.15 K/mm) and with a constant temperature gradient ($G = 5.15$ K/mm) in a wide range of growth rates (8.3–500 μm/s) with a Bridgman-type directional solidification furnace. The microhardness (HV) and tensile strength (σ) of alloy were measured from directionally solidified samples. The dependency of the microhardness, tensile strength for directionally solidified Zn–1.26 wt% Al alloy on the solidification parameters (G, V) and microstructure parameters (λ_1, λ_2) were investigated and the relationships between them were experimentally obtained using regression analysis. According to present results, the microhardness and tensile strength of directionally solidified Zn–1.26 wt% Al alloy increase with increasing solidification processing parameters and decrease with the microstructure parameters. Variations of electrical resistivity (ρ) with the temperature in the range of 300–650 K were also measured using a standard dc four-point probe technique for cast samples. The enthalpy of fusion and specific heat for same alloy was also determined by means of differential scanning calorimeter (DSC) from heating trace during the transformation from solid to liquid.

Introduction

Dendritic structures are frequently observed during the solidification of alloys. The presence of dendritic structures during solidification, with concomitant microsegregations, is of great interest since these solidification features are commonly found in many engineering materials and furthermore, greatly influence the mechanical behavior [1, 2]. Many researchers have developed different types of alloys, such as aluminium-based alloys, zinc-based alloys, copper-based alloys, bearing bronzes, and cast iron used in various engineering applications [3–10]. Among these alloy systems, zinc-based alloys have several advantages over other commonly used casting alloys based on iron, aluminum, or copper. Compared to cast iron, the zinc-based alloys have better machinability, can be cast to closer tolerances, and have a superior as-cast surface finish. In addition, compared to aluminum and copper, these alloys are harder and stronger, machine more easily, have superior pressure tightness, and have substantially better wear and bearing characteristics [11–14]. They are also used in many applications, including portable computers, radiofrequency circuits, transformer cores, and many other electrical and electronics consumer applications [15–18]. The effect of microstructure on zinc-aluminium alloys properties has been highlighted in various studies and particularly, the influence of growth rate and dendrite arm spacing upon the mechanical properties and corrosion resistance has been reported [19–21].

The aims of present study were to study the dependency of microhardness, tensile strength on the solidification processing parameters (G and V), and microstructure parameters (λ_1, λ_2) for directionally solidified Zn–1.26 wt% Al alloy and the variation of electrical resistivity of this alloy as a function of temperature (300–650 K) and growth rate (8.3–500 μm/s). This composition of the alloy has been especially chosen since it permits for the formation of a fine dendritic structure.

E. Çadırlı (✉) · M. Şahin
Department of Physics, Faculty of Arts and Sciences, Niğde University, Niğde, Turkey
e-mail: ecadirli@gmail.com

Experimental details

The Zn–1.26 wt% Al alloy bulk samples were prepared by melting weighed quantities of Zn and Al (high purity >99.99%) in a graphite crucible placed into a vacuum melting furnace. After allowing time for the melt to become homogeneous, the molten alloy was poured into ten graphite crucibles (250 mm in length 4 mm ID and 6.35 mm OD) in a hot filling furnace. Each sample was than positioned in a Bridgman-type furnace (see Fig. 1) in a graphite cylinder (300 mm in length 10 mm ID and 40 mm OD). After stabilizing the thermal conditions in the furnace under an argon atmosphere, the sample was grown by pulling downwards at a constant rate by means of a synchronous motor. Samples were solidified under steady-state conditions [3, 22–24] with a constant growth rate (16.6 μm/s) at the different temperature gradients (1.94–5.15 K/mm), and with a constant temperature gradient (5.15 K/mm) in a wide range of growth rates (8.3–500 μm/s).

Measurement of solidification processing parameters (*G*, *V*)

In directional solidification experiments, solidification parameters (G, V) may be independently controlled so that one may study the dependence of microstructural parameters on either G at constant V, or V at constant G for the constant alloy composition C_0. The temperature of the Bridgman-type furnace was controlled to an accuracy of ±0.1 K with a *Eurotherm 2604* type controller. The temperatures in the sample were measured with K type 0.25 mm in diameter insulated two thermocouples fixed within the sample with spacing of 10 mm. Accuracy of the thermocouples which are placed in the sample both perpendicular and parallel to the heat flow direction was checked by slowly solidifying the sample. The temperature difference measured using the thermocouples at the melting point ($T_m \sim 655$ K) of this studied alloy is less than 0.5 K. In this study, a 1.2 mm OD × 0.8 mm ID alumina sheaths were used to insulate the thermocouples from the

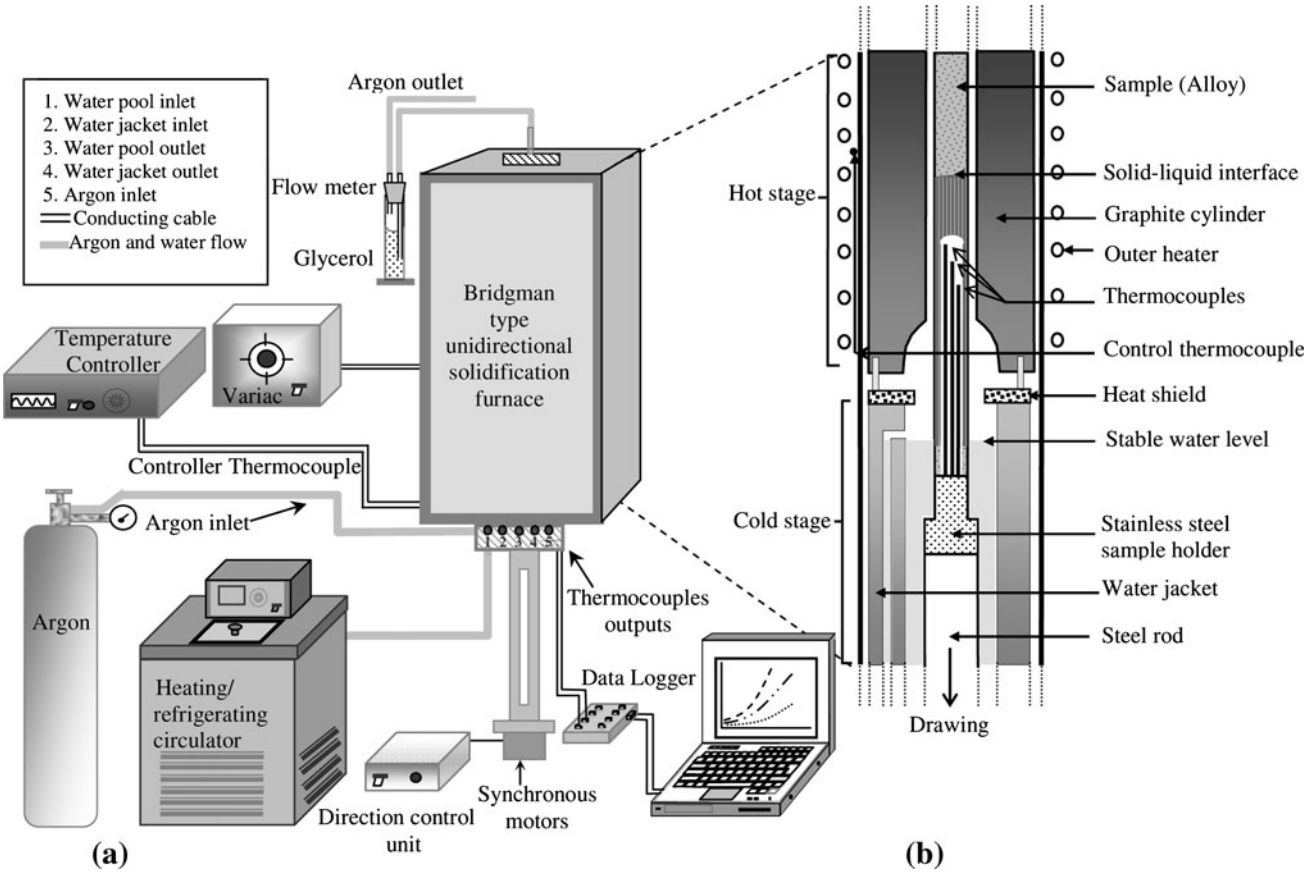

Fig. 1 **a** Block diagram of the experimental setup, and **b** the details of the Bridgman-type directional solidification furnace

melts. Before inserting the thermocouples into the alumina sheath, the distance (ΔX) between the thermocouples was determined by measuring the length of these alumina sheaths. Thermocouples readings (at intervals of 0.5 s) were collected by a data-logger system and stored on a computer.

When the second thermocouple was at the solid–liquid interface (temperature of solid phase, T_S) and the first thermocouple in the liquid (temperature of liquid phase, T_L), their temperatures were used to determine G values. The temperatures of the liquid phases for each sample were 675.3, 682.2, 687.9, 696.7, and 707.5 K, respectively, and temperature of solid phase (T_S) was 656 K. The temperature gradient ($G = \Delta T/\Delta X = T_L - T_S/X_L - X_S$) for each sample was determined using the measured value of ΔT and the known value of ΔX.

The growth rate was calculated with two different methods. In the first method, the values for the growth rate were calculated from the measurements of the time taken for the solid/liquid interface to pass the thermocouples separated by a known distance. In the second method, solidification time and solidification distance (on the longitudinal section of the polished sample) were measured. The ratios ($V = \Delta X/\Delta t$) of the distances to the times were measured to obtain the growth rates and these were similar for both methods.

Metallographic process and measurement of microstructure parameters (λ_1, λ_2)

The quenched samples were removed from the graphite crucibles and cut into lengths typically 20 mm. The longitudinal and transverse sections were ground flat with 180, 500, 1000, 2500 grit SiC paper, and polished using 6, 3, 1, 0.25, 0.05 μm diamond paste. The longitudinal and transverse sections of ground sample were then cold mounted with epoxy-resin. After polishing, the samples were etched with an etching solution (40 g CrO_3, 1.5 g Na_2SO_4, 200 mL H_2O) for 5 s. After metallographic process, the microstructures of the samples were revealed. As can be seen from Fig. 2, dendritic microstructure was observed for Zn–1.26 wt% Al alloy.

The primary dendrite arm spacings (PDAS), λ_1 was obtained by measuring the distance between the nearest two dendrites trunks (see Fig. 2). Two different methods were used to measure the λ_1 values on the transverse sections. The first method is the triangle method [25]. The triangle is formed by joining the three neighboring dendrite

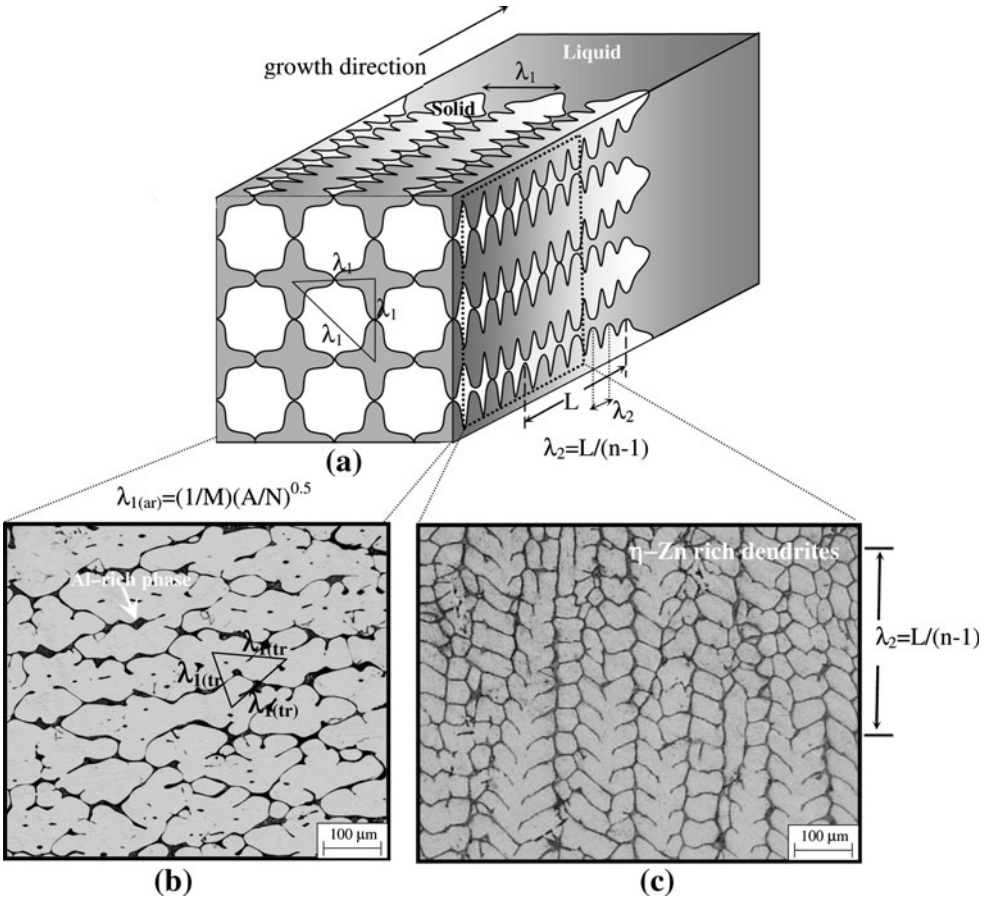

Fig. 2 **a** Schematic illustration of the microstructure parameter measurements, **b** measurement of λ_1 with the triangle and area counting methods on the transverse section, and **c** measurements of λ_2 on the longitudinal section

centres, and the sides of triangle corresponded to $\lambda_{1(tr)}$. The second method is the area counting method [26]. The values of $\lambda_{1(ar)}$ were measured on the cross section of sample (see Fig. 2). In this method the average primary dendrite arm spacings, $\lambda_{1(ar)}$ were determined from

$$\lambda_{1(ar)} = \frac{1}{M}\left(\frac{A}{N}\right)^{0.5} \quad (1)$$

where M is the magnification factor, A is the total sample cross sectional area, and N is the number of primary dendrites on the crossection. λ_1 is the arithmetic average values of $\lambda_{1(tr)}$ and $\lambda_{1(ar)}$. The secondary dendrite arm spacings (SDAS), λ_2 were measured by averaging the distance between adjacent side branches on the longitudinal section of a primary dendrite. Each of side-branch spacings data reported here is the average of the initial λ_2 values from 5–10 primary dendrites for each sample. For each G and V, numerous measurements related to the microstructure parameters were measured to increase statistical reliability. Thus, the values of λ_1 and λ_2 were measured as a function of G and V for the Zn–1.26 wt% Al system.

Measurement of microhardness (HV)

One of the purposes of this investigation was to obtain the relationships between solidification processing parameters (G and V), microstructure parameters (λ_1, λ_2), and microhardness hardness (HV) for the directionally solidified Zn–1.26 wt% Al alloy. The mechanical properties of any solidified materials are usually determined with hardness test, tensile strength test, ductility test, etc. The Vickers hardness (HV) is the ratio of a load applied to the indenter to the surface area of the indentation. This is given by

$$\mathrm{HV} = \frac{2P\sin(\theta/2)}{d^2} \quad (2)$$

where HV is the Vickers microhardness in kg/mm^2, P is the applied load (kg), d is the mean diagonal of the indentation (mm), θ is the angle between opposite faces of the diagonal indenter (136^o). Microhardness measurements of the samples in this study were made with a *Future-Tech FM-700* model hardness measuring test device using a 10–50 g load and a dwell time of 10 s giving a typical indentation depth about 40–60 μm. The microhardness was the average of at least 30 measurements made on the sample.

Measurement of tensile strength (σ)

The uniaxial tensile tests were performed at room temperature at a strain rate of 10^{-3} s^{-1} with a *Shimadzu Universal Testing Instrument* (Type AG-10KNG), which was designed for testing the stress–strain responses of solders. In order to avoid damaging the sample surface, two seals were stuck on the sample instead of the traditional clip gauge. Strains were then measured by observing the displacement between the two seals using a video camera. A computer with data acquisition software was used to collect the data. The data collected from the tensile test can be analysed using the following formula to determine the strength (σ).

$$\sigma = \frac{F}{A} \quad (3)$$

where σ is the strength in N/mm^2 (or MPa), F is the applied force (N), A is the original cross sectional area (mm^2) of the sample. The round rod tensile samples with diameter of 4 mm and gauge length of 20 mm were prepared from directionally solidified rod samples with different solidification parameters. The tensile axis was chosen parallel to the growth direction of the sample and the tests were repeated three times. It has been found that a standard deviation is approximately 5%.

The measurement of electrical and thermal properties of the alloy

Other purposes of this study were to obtain measurements of the electrical and thermal properties in the Zn–1.26 wt% Al alloy such as electrical resistivity (ρ), enthalpy (ΔH), and specific heat (C_p). The temperature and growth rate dependence of electrical resistivity for Zn–1.26 wt% Al alloy were measured by the four-point probe method [27]. Today the four-point probe method is the most widely used technique for measuring the electrical profile of materials. In this method, the material's resistivity, ρ, can be calculated by the relation $\rho = \mathrm{RCF}\ (V_{measured}/I_{measured})$. The resistivity correction factor (RCF) takes the size of the test structure, the thickness of the material, the size of the electrodes, and the position of the electrodes with respect to the boundary of the test structure, into account [28]. A *Keithley 2400* sourcemeter was used to provide constant current, and the potential drop was measured by a *Keithley 2700* multimeter through an interface card, which was controlled by a computer. Platinum wires with a diameter of 0.5 mm were used as current and potential probes. The voltage drop was detected, and the electrical resistivity and conductivity were determined using a standard conversion method. Measurements were made in the temperature range of 300–650 K. The temperature of the sample was adjusted by a controllable *Nabertherm P320* heater, and the temperature of the sample was measured using a standard K-type thermocouple which was placed near the samples. The sample dimensions (approximately 12 mm in length, 4 mm in diameter) were measured to an accuracy of 1 μm using a digital micrometer. The resistance data were converted to resistivity values with the measured sample

dimensions. The details of the measuring method have been described elsewhere [29].

The electrical resistivity strongly depends on the temperature. In metals, electrical resistivity increases with increasing temperature. The temperature coefficient of resistivity (α) in K^{-1} units is often expressed as a slope in the electrical resistivity versus temperature graph and can be given as

$$\alpha = \frac{\rho_S - \rho_{S0}}{\rho_{S0}(T - T_0)} = \frac{1}{\rho_{S0}}\frac{\Delta\rho}{\Delta T} \quad (4)$$

where ρ_s is the electrical resistivity at the temperature T and ρ_{s0} is the electrical resistivity at the room temperature, $T_0 = 300$ K. The growth rate dependence of the electrical resistivity was also measured at the room temperature for Zn–1.26 wt% Al alloy.

The enthalpy (ΔH) and the specific heat (C_p) of Zn–1.26 wt% Al alloy ($\sim$10 mg) were determined because they are very important parameters for industrial applications. DSC thermal analysis (*Perkin Elmer Diamond model*) was performed in the temperature range from room temperature to 790 K at a heating rate of 10 K/min under a constant stream of nitrogen at atmospheric pressure. We used a reference material (a sapphire disk) in determining specific heat. This reference data is used to "correct" sample data at every temperature. The size of the signal which is used to calculate the specific heat is proportional to the heating rate, so it follows that faster heating rates will produce larger signals, which would give more accurate data. However, if the heating rate is too high, the temperature gradients in the sample will be large and this may introduce other errors in the measurement. It is normal to use heating rates between 5 and 20 K/min. The heating rate in this study was 10 K/min, which is mostly recommended. The enthalpy of fusion (ΔH) was calculated as the area under the peak by numerical integration. The difference between the sample curve and the baseline curve is measured in milliwatts, and converted to specific heat as follows [30],

$$C_p = \frac{dQ}{dt}\frac{1}{m\beta} \quad (5)$$

where dQ/dt is heat flow, m is the mass of the sample, and β is the heating rate in K/min.

Results

The microstructure and composition analysis of phases

The microstructures of samples were characterized from both transverse and longitudinal sections using an *Olympus BX-51* optical microscopy. The microstructure of Zn–1.26 wt% Al alloy consists of coarse η-Zn rich dendrites. It can be seen from Fig. 2, the Zn-rich matrix phase appears gray and Al-rich phase appears dark.

The maximum solubility of Al in Zn is 1.17 $\pm$ 0.08 wt% (98.83 wt% Zn) at the eutectic temperature, decreasing to 0.67 at.% (99.33 wt% Zn) at 550 K, and 0.03 (99.97 wt% Zn) at 293 K [31]. EDX analysis was performed to determine nominal composition of alloy. The EDX analysis was carried out at 20 keV using the X-ray lines. A typical EDX analysis is shown in Fig. 3. As can be seen from Fig. 3, the composition of the casting phase was also found to be Zn–1.26 wt% Al (or Zn–3 at.% Al). Also, this value was confirmed by wavelength dispersive X-ray fluorescence spectrometry (WDXRF).

Dependency of the microhardness on the solidification and microstructure parameters

One of the purposes of this investigation was to obtain the relationships among G, V, λ_1, λ_2, and HV for the directionally solidified Zn–1.26 wt% Al alloy. The variations of microhardness with the solidification and microstructure parameters are plotted and given in Figs. 4–6. As can be seen from Figs. 4–6, the dependence of HV on G, V, λ_1, and λ_2 can be expressed by the following equations as,

$$HV = k_i G^a \text{ (at a constant } V) \quad (6a)$$

$$HV = k_i V^b \text{ (at a constant } G) \quad (6b)$$

$$HV = k_i \lambda_1^{-c} \quad (6c)$$

$$HV = k_i \lambda_2^{-d} \quad (6d)$$

where k_i is a constant, a, b, c, and d are the exponent values relating to the temperature gradient, growth rate, PDAS and SDAS, respectively. As can be seen from Fig. 4, the microhardness values increase with the increasing G for a given constant growth rate (V). It is found that increasing temperature gradient from 1.94 to 5.15 K/mm, microhardness increases from 52.6 to 66.7 kg/mm^2. The value of the

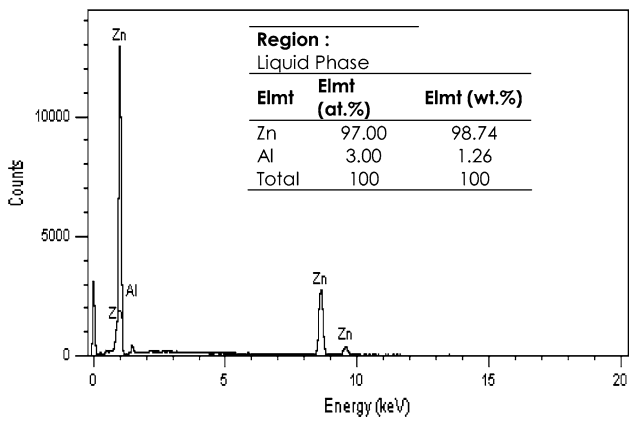

Fig. 3 Typical EDX results for Zn–1.26 wt% Al alloy

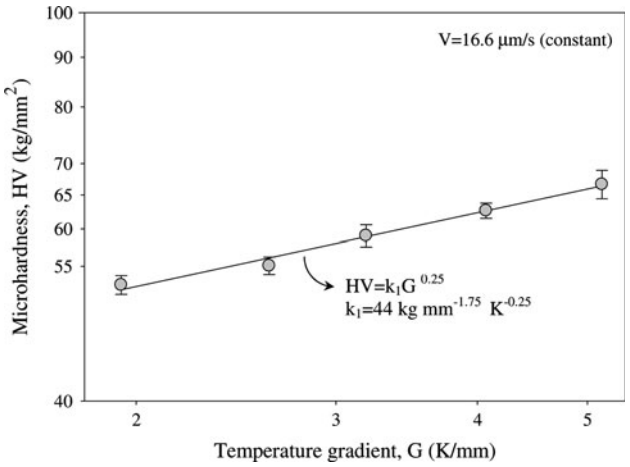

Fig. 4 Variation of the microhardness with the temperature gradient

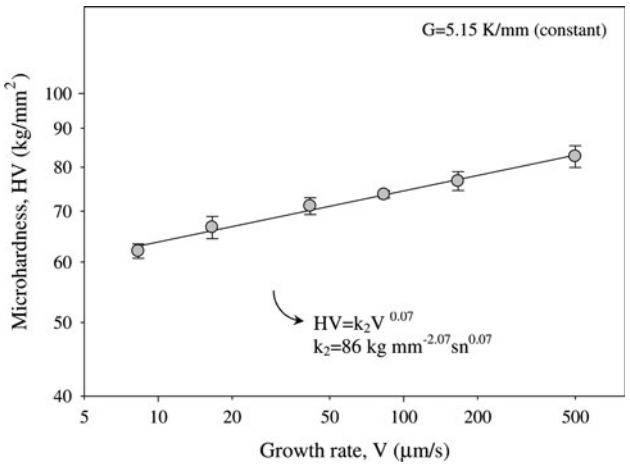

Fig. 5 Variation of the microhardness with the growth rate

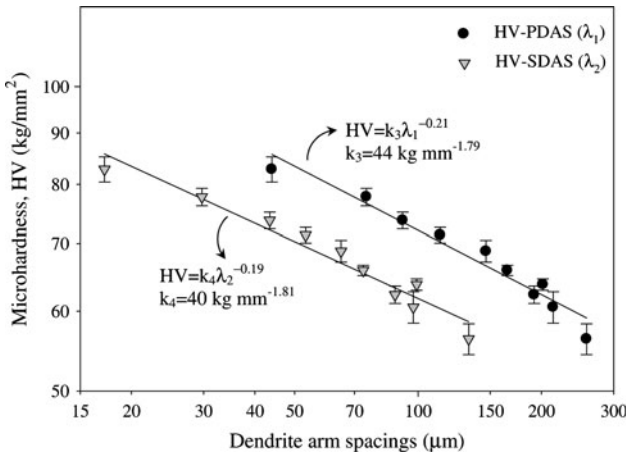

Fig. 6 Variation of the microhardness with dendrite spacings

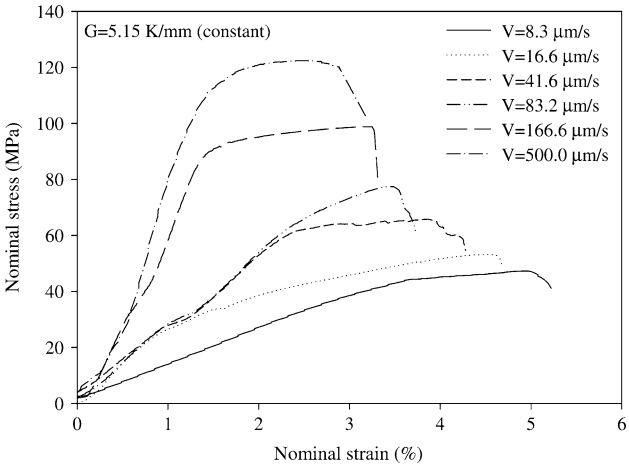

Fig. 7 Typical nominal stress–strain curves for unidirectional solidified Zn–1.26 wt% Al alloy under certain solidification condition

exponent relating to the temperature gradient (G) is equal to 0.25 for unidirectional solidified Zn–1.26 wt% Al alloy.

Figure 5 shows the variation of HV as a function of V at a constant G. The value of HV increases with the increasing value of V. It is found that increasing growth rate from 8.3 to 500 μm/s, the values of microhardness increase from 62.1 to 82.7 kg/mm^2.

The variations of the microhardness as a function of the PDAS and SDAS are given in Fig. 6 for the Zn–1.26 wt% Al alloy. It can be observed that a decrease in PDAS and SDAS values leads to increase in the HV values, from 56.3 to 82.8 kg/mm^2.

Dependency of the ultimate tensile strength (σ) on the solidification and microstructure parameters

Another aim of this study was to obtain the relationships among σ with G, V, and λ_2 in the Zn–1.26 wt% Al alloy. The typical nominal stress–strain curves of Zn–1.26 wt% Al alloy under different growth rates at a constant temperature gradient (5.15 K/mm) and strain rate ($\sim 10^{-3}$ s^{-1}) are shown in Fig. 7. Figure 7 shows the influence of growth rate on the stress at a constant temperature gradient. At a constant strain rate of 10^{-3} s^{-1}, the alloy hardens continuously and the stress increases as the growth rate increases.

The dependence of σ on the G, V, λ_1, and λ_2 can be represented by equations as following,

$$\sigma = k_i G^m \text{ (at a constant } V) \quad (7a)$$

$$\sigma = k_i V^n \text{ (at a constant } G) \quad (7b)$$

$$\sigma = k_i \lambda_2^{-p} \quad (7c)$$

where k_i is a constant, m, n, and p are the exponent values relating to the G, V, and λ_2, respectively. Figures 8–10 show the results of the UTS (σ) as a function of temperature gradient (G), growth rate (V), and secondary dendrite arm spacing (λ_2) for Zn–1.26 wt% Al alloy. Figure 8 shows

the experimental results of σ as a function of G. As seen from this figure, it is found that when increasing temperature gradient from 1.94 to 5.15 K/mm, mean ultimate tensile strength increases from 41.3 to 53.2 MPa. The ultimate tensile strength increased 28%. The value of the exponent relating to G is equal to 0.25 for UTS.

Figure 9 shows the variation of σ as a function of V. And also it can be seen that value of σ increases with the increasing growth rate. It is found that the UTS increases from 47.3 to 122.5 MPa, when growth rate increasing from 8.3 to 500 μm/s. The value of the exponent relating to the growth rate is equal to 0.24 for UTS. Temperature gradient and growth rate have a strong impact on ultimate tensile strength.

Figure 10 shows the experimental results of UTS as a function of SDAS. It can be seen that UTS increase with decreasing SDAS. It is found that the UTS increases from 41.3 to 122.5 MPa, when SDAS decreasing from 133 to 17 μm. The value of the exponent relating to the SDAS was obtained to be 0.59.

The electrical and thermal properties of Zn–1.26 wt% Al alloy

As mentioned above, the variation of electrical resistivity (ρ) with the temperature in the range of 300–650 K for Zn–1.26 wt% Al cast alloy were measured and plotted as shown in Fig. 11. As can be seen from Fig. 11, the values of ρ were found to be in the range of 3.8×10^{-8}–14×10^{-8} Ω m. Figure 11 shows that the resistivity increases linearly with the increasing temperature, which is typical metallic behavior [27]. The temperature coefficients of electrical resistivity (α) for Zn–1.26 wt% Al alloy was determined to be 7.96×10^{-3} K^{-1} from the graph of

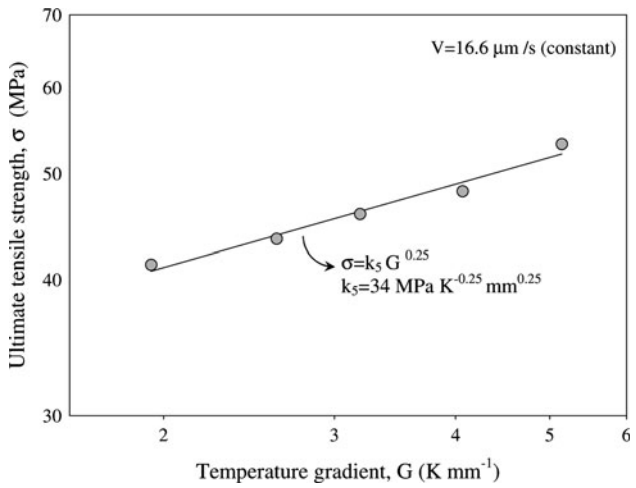

Fig. 8 Variation of the ultimate tensile strength with the temperature gradient

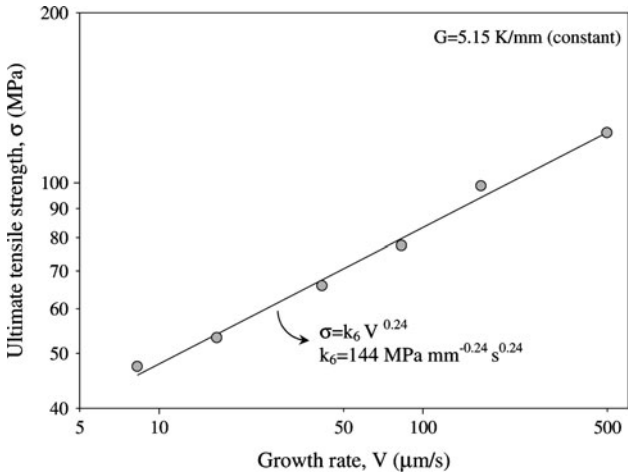

Fig. 9 Variation of the ultimate tensile strength with the growth rate

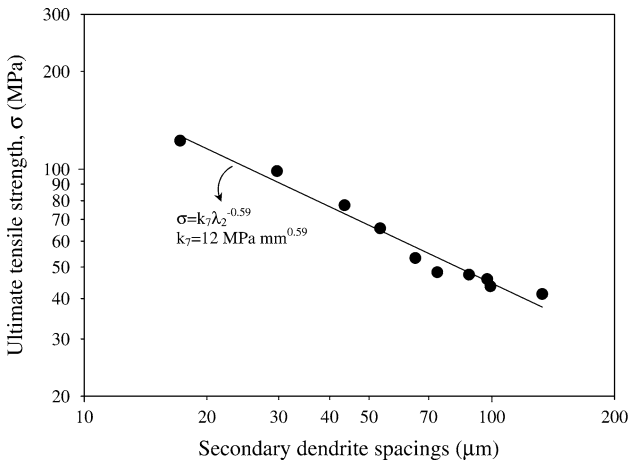

Fig. 10 Variation of the ultimate tensile strength with secondary dendrite spacings

electrical resistivity variation versus temperature. The α value (7.96×10^{-3} K^{-1}) is bigger than the value 4.95×10^{-3} K^{-1} obtained by Böyük et al. [32] for Zn–1.5 Cu alloy. The variation of the resistivity as a function of the growth rate is given in Fig. 12 for the Zn–1.26 wt% Al alloy. It can be observed that an increase in growth rate values leads to increase in the resistivity values from 5.2×10^{-8} to 6.7×10^{-8} Ω m.

The Zn–1.26 wt% Al alloy was heated at a rate of 10 K/min from the room temperature to 790 K using a Perkin Elmer Diamond model DSC and the heat flow versus temperature is given in Fig. 13. It is clear that sharp peak is observed for melting process and the melting temperature of Zn–1.26 wt% Al alloy was detected to be 658.9 K. The values of the enthalpy of fusion (ΔH) and the specific heat (C_p) for Zn–1.26 wt% Al alloy were also calculated to be 113.4 J/g and 0.294 J/g K, respectively, from the graph of the heat flow versus temperature.

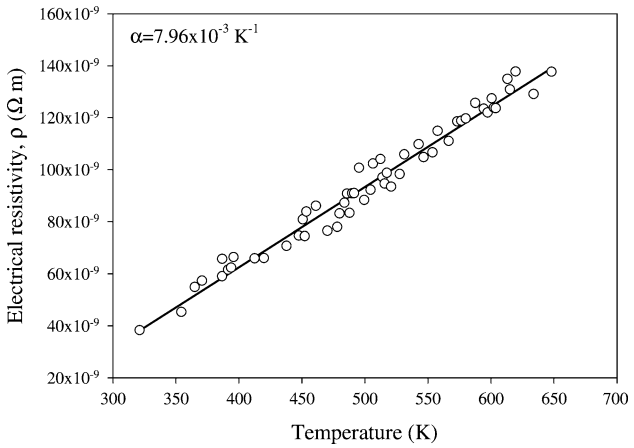

Fig. 11 Temperature dependence of the electrical resistivity for Zn–1.26 wt% Al cast alloy

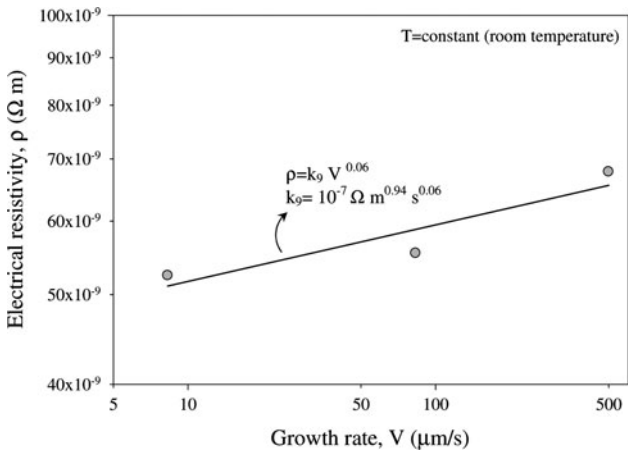

Fig. 12 Variation of the electrical resistivity as a function of growth rate at the room temperature

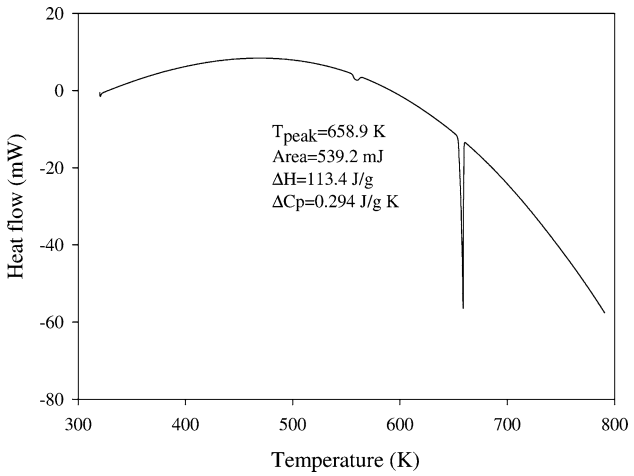

Fig. 13 Heat flow curve versus the temperature for Zn–1.26 wt% Al alloy with a heating rate of 10 K/min

Discussion

As can be seen from Fig. 4, the exponent value (0.25) relating to G obtained in this study is generally in a good agreement with the exponent values relating to the G obtained in previous experimental studies [33, 34]. The exponent value relating to the growth rate obtained in this study is found to be 0.07 and close to 0.07, 0.08, and 0.10 obtained by Vnuk et al. [35, 36], and Telli and Kısakürek [37] for different eutectic alloys. These values of HV are fairly bigger than the values obtained by Rosenberger et al. [38] for Zn–1 wt% Al and Zn–2 wt% Al alloys. The values of the exponent relating to the PDAS and SDAS were obtained to be 0.21 and 0.19, respectively. These exponent values relating to the dendrite spacings are close to the values of 0.20, 0.21, 0.22, 0.18, and 0.22 obtained by Kaya et al. [39] for Pb–Cd, Sn–Zn, Bi–Cd, Kaya et al.[40] for Al–Si, and Khan et al. [41] for Al–Si, respectively. However, the exponent values relating to the dendrite spacings obtained in this study are quite smaller than the values of 0.50 by Telli and Kısakürek [37].

The maximum value of UTS of 122.5 MPa obtained in this study is smaller than 154 MPa value obtained by Osorio and Garcia [42] for Zn–3 wt% Al alloy under unsteady-state conditions. One of the causes of this is the amount of aluminum in the alloy, because aluminium is an important factor on the ultimate tensile strength for Zn–Al alloys. Another factor is the differences in growth rate. The growth rate values (8.3–500 μm/s) in this study are smaller than the growth rate values (400–1500 μm/s) obtained by Osorio and Garcia [42] under unsteady-state conditions. The exponent value (0.59) relating to the SDAS is slightly bigger than the value of 0.50 obtained by Osorio and Garcia [42] and Santos et al. [21] for Zn–3 wt% Al and Zn–27 wt% Al alloys, respectively.

Besides temperature, the effect of the growth rate on the electrical resistivity also was observed. It can be observed that an increase in growth rate values leads to increase in the resistivity values from 5.2×10^{-8} to 6.7×10^{-8} Ω m. The reason for this might be that the increased growth rate caused a reduction in grain size. Consequently, carrier scattering at the increased density of grain boundaries would cause additional resistivity.

The ΔH value (113.4 J/g) calculated in this study are in a good agreement with the values 115.7 and 118.4 J/g obtained by Osorio and Garcia [42] for Zn–1 wt% Al alloy and Ares and Schvezov [43] for Zn–2 wt% Al alloy, respectively. These results are only 2–4% larger than this study. For the experimental measurement, there is always 5–10% error. It is obvious that the difference among the three calculated results is smaller than the experimental error. Besides, the value (397.1 J/g) obtained by Feng et al. [44] for Zn–0.53 wt% Al alloy is fairly bigger than the

value of ΔH in this study. One reason for this difference might be small difference of the composition for the studied alloys. Another possible reason is that, Feng et al. [44] have performed under rapid solidification conditions. Also, the sample mass, heating, and cooling rate effects should also be ignored.

Conclusions

In this study, the influence of solidification processing parameters (G, V) and microstructure parameters (λ_1, λ_2) on the microhardness and ultimate tensile strength of Zn–1.26 wt% Al alloy were investigated. Also, some electrical (ρ, σ) and thermal properties (ΔH, Cp) of this alloy were investigated. The results are summarized as follows;

1. The values of HV for directionally solidified Zn–1.26 wt% Al alloy have been measured at at least 30 regions on the sample. It was found that the values of microhardness (HV) increase with increasing the values of G and V and decrease with increasing λ_1 and λ_2 values. The establishment of the relationships among HV, G, V, λ_1, and λ_2 can be given as

$$\mathrm{HV} = k_1 G^{0.25}, \mathrm{HV} = k_2 V^{0.07}, \ \mathrm{HV} = k_3 \lambda_1^{-0.21}, \text{ and } \mathrm{HV} = k_4 \lambda_2^{-0.19}$$

   where the exponent values relating to the G, V, λ_1, and λ_2 are 0.25, 0.07, 0.21, and 0.19, respectively. These exponent values agree very well with the exponent values relating to G, V, λ_1, and λ_2 obtained in previous studies [33–37, 39–41].
2. The experimental expressions correlating the values of σ with the values of G, V, and λ_2 for directionally solidified Zn–1.26 wt% Al alloy have shown that the values of the tensile strength increase with increasing the values of G and V and decrease with increasing λ_2 values. The establishment of the relationships among σ, G, V, and λ_2 can be given as

$$\sigma = k_5 G^{0.25}, \ \sigma = k_6 V^{0.24}, \text{ and } \sigma = k_7 \lambda_2^{-0.59}$$

   where the exponent values relating to the G, V, λ_1, and λ_2 are 0.25, 0.24, and 0.59 for tensile strength. The maximum value of tensile strength of 122.5 MPa obtained in this study is smaller than 154 MPa value obtained by Osorio and Garcia [42].
3. The electrical resistivity (ρ) of Zn–1.26 wt% Al cast alloy increased with the increasing temperature from 3.8×10^{-8} to 14×10^{-8} Ω m. The temperature coefficient of electrical resistivity was determined to be 7.96×10^{-3} K^{-1} from the graph of electrical resistivity variation versus temperature. The growth rate is also influenced on the resistivity at room temperature. The value of ρ slightly increases from 5.2×10^{-8} to 6.7×10^{-8} Ω m with the increasing growth rate.
4. The Zn–1.26 wt% Al alloy was heated at a rate of 10 K/min from room temperature to 790 K. From the trace of heat flow versus temperature, the melting temperature of Zn–1.26 Al alloy was detected to be 658.9 K. The values of the enthalpy of fusion (ΔH) and the specific heat (C_p) for Zn–1.26 Al cast alloy were found to be 113.4 J/g and 0.294 J/g K, respectively.

Acknowledgements This project was supported by the Niğde University Scientific Research Project Unit under Contract No: FEB 2009/02. Authors would like to thank to the Niğde University Scientific Research Project Unit for their financial support.

References

1. Yılmaz F, Elliott R (1989) J Mater Sci 24:2065. doi:10.1007/BF02385422
2. Grugel RN (1995) Metall Mater Trans A 26:496
3. Çadırlı E, Gündüz M (2000) J Mater Sci 35:3837. doi:10.1023/A:1004829413966
4. Mullis AM (2003) J Mater Sci 38:2517. doi:10.1023/A:1023977723475
5. Li L, Zhang Y, Esling C, Zhao Z, Zuo Y, Zhang H, Cui J (2009) J Mater Sci 44:1063. doi:10.1007/s10853-008-3158-0
6. Kumar A, Dutta P (2009) J Mater Sci 44:3952. doi:10.1007/s10853-009-3539-z
7. Pandey JP, Prasad BK (1998) Metall Mater Trans A 29:1245
8. Calayag TS (1986) Zinc–aluminium (ZA) cast alloys. Proc Int Symp CIM, Toronto
9. Zhu YH, Man HC, Dorantes-Rosales HJ, Lee WB (2003) J Mater Sci 38:2925. doi:10.1023/A:1024457109307
10. Abou El-khair MT, Daoud A, Ismail A (2004) Mater Lett 58:1754
11. Ravindranathan P, Patil KC (1987) J Mater Sci 22:3261. doi:10.1007/BF01161190
12. Zhu Y, Yan B, Huang W (1995) J Mater Sci Tech 11:109
13. Hung FY, Lui TS, Chen LH, You JG (2007) J Mater Sci 42:3865. doi:10.1007/s10853-006-0463-3
14. Krupinska B, Dobrzanski LA, Rdzawski ZM, Labisz K (2010) Arch Mater Sci Eng 43:13
15. Morgan SWK (1985) Zinc and its alloys and compounds. Wiley, New York
16. Flores OV, Kennedy C, Murr LE, Brown D, Pappu S, Nowak BM, McClure JC (1998) Scr Mater 38:703
17. Park HS, Kimura T, Murakami T, Nagano Y, Nakata K, Ushio M (2004) Mater Sci Eng A 371:160
18. Pürcek G (2005) J Mater Process Technol 169:242
19. Osorio WR, Freire CM, Garcia A (2005) J Mater Sci 40:4493. doi:10.1007/s10853-005-0852-z
20. Osorio WR, Freire CM, Garcia A (2005) J Alloys Compd 397:179
21. Santos GA, Neto CM, Osorio WR, Garcia A (2007) Mater Des 28:2425
22. Ding GL, Tewari SN (2002) J Cryst Growth 236:42
23. Hui J, Tiwari R, Wu X, Tewari SN, Trivedi R (2002) Metall Mater Trans A 33:3499
24. Feng J, Huang WD, Lin X, Pan QY, Li T, Zhou YH (1999) J Cryst Growth 197:393

25. Ganesan S, Chan CL, Poirier DR (1992) Mater Sci Eng A 151:97
26. Bhat MS, Poirier DR, Heinrich JC (1995) Metall Mater Trans B 26:1049
27. Smiths FM (1958) Bell Syst Tech J 37:711
28. Valdes LB (1954) Proc IRE 42:420
29. Arı M, Saatçi B, Gündüz M, Meydaneri F, Bozoklu M (2008) Mater Charact 59:624
30. Robinson P (2003) Practical specific heat determination by power compensation DSC. Perkin Elmer, Seer Gren
31. Massalski TB (ed) (1990) Binary alloy phase diagrams, vol 3. ASM International, Materials Park
32. Böyük U, Kaya H, Çadırlı E, Maraşlı N, Ülgen A (2010) J Alloys Compd 491:143
33. Kaya H, Çadırlı E, Böyük U, Maraşlı N (2008) App Surf Sci 255:307
34. Kaya H, Böyük U, Çadırlı E, Ocak Y, Akbulut S, Keşlioğlu K, Maraşlı N (2008) Met Mater Int 14:575
35. Vnuk F, Sahoo M, Van De Merwe R, Smith RW (1979) J Mater Sci 14:975. doi:10.1007/BF00550730
36. Vnuk F, Sahoo M, Baragor D, Smith RW (1980) J Mater Sci 15:2573. doi:10.1007/BF00550762
37. Telli AI, Kısakürek SE (1988) Mater Sci Technol 4:153
38. Rosenberger MR, Ares AE, Gatti IP, Schvezov CE (2010) Wear 268:1533
39. Kaya H, Gündüz M, Çadırlı E, Uzun O (2004) J Mater Sci 39:6571. doi:10.1023/B:JMSC.0000044897.98694.be
40. Kaya H, Çadırlı E, Gündüz M, Ülgen A (2003) J Mater Eng Perform 12:544
41. Khan S, Ourdjini A, Hamed QS, Najafabadi MAA, Elliott R (1993) J Mater Sci 28:5957. doi:10.1007/BF00365208
42. Osorio WR, Garcia A (2002) Mater Sci Eng A 325:103
43. Ares AE, Schvezov CE (2007) Metall Mater Trans A 38:1485
44. Feng J, Huang WD, Lin X, Pan QY, Li T, Zhou YH (1999) J Mater Sci Lett 18:29